Experimental Characterization of Structural Features during Radical Chain Homopolymerization of Multifunctional Monomers Prior to Macroscopic Gelation

J. Brian Hutchison,[†] Alex S. Lindquist,[†] and Kristi S. Anseth*[,†,‡]

Department of Chemical and Biological Engineering, University of Colorado, Boulder, Colorado 80309-0424, and Howard Hughes Medical Institute, University of Colorado, Boulder, Colorado 80309-0424

Received September 18, 2003; Revised Manuscript Received March 22, 2004

ABSTRACT: An experimental methodology is presented to characterize the evolution of structural heterogeneities in cross-linked polymer networks formed by homopolymerizations of multifunctional monomers. In particular, intramolecularly cross-linked macromolecules (ICMs) were synthesized by individual initiation events and characterized. A set of complementary experimental tools, including atomic force microscopy (AFM), size exclusion chromatography, light scattering, and NMR, is used to provide information about size, intramolecular cross-link density, and kinetic chain length for poly(methacrylic anhydride) (PMA) ICMs. Images of PMA ICMs, which contain ca. 1000−2000 monomers, on average, are captured with AFM. Varying polymerization temperature from −13 to 70 °C led to an increase in the apparent size of the ICMs and an increase in the fraction of doubly reacted monomers. Furthermore, ICMs synthesized in the presence of tetraethylthiuram disulfide (TED), a photoiniferter precursor, were characterized. Iniferter-mediated polymerization of methacrylic anhydride created smaller ICMs with higher intramolecular cross-link density.

Introduction

Investigations of Structural Evolution. The development of heterogeneity during the evolution of highly cross-linked networks from homopolymerizations of multifunctional monomers impacts many applications and is an important area of research.[1−12] Current commercial applications of multifunctional monomers that would benefit from a better understanding of their cross-linked network structural evolution include abrasion-resistant coatings, dental materials, and flexographic printing plates, among others. A more complete understanding of nanoscale evolution of polymeric materials is critically important for their implementation in microelectronics and microdevice technologies as well as higher resolution applications such as molecular templating,[13,14] data storage, and quantum computing that necessitate nanoscale control and functionality.

The size and structure of the heterogeneous regions, along with relationships to the monomer structure and initiation conditions, are not well understood or characterized. With a better understanding of reaction and reactant parameters that influence structural evolution during multifunctional monomer polymerizations, opportunities exist to control and enhance the structure and properties of the resulting macroscopic networks.

While researchers are making significant progress in this area, most results provide indirect measures of heterogeneous structure evolution. For example, regions of more highly cross-linked polymer within an evolving network have been attributed to enhanced reactivity of functional groups near sites of active radicals.[1,2] The same phenomenon can lead to trapping of propagating radicals within highly cross-linked regions—microgels.[3,15] Although the small size of the heterogeneous regions precludes the use of spectroscopic techniques or visible light microscopies, information about the development of heterogeneity in multifunctional monomer polymerizations has been obtained via electron microscopy,[6] film surface ablation,[16] mechanical property measurements,[10,17] and fluorescence and NMR spectroscopies.[12,18−20] Finally, a body of information, gathered from simulations of cross-linked network evolution, has provided substantial insight into structural evolution.[2,3,5,6,12,21,22] However, the rich information available from a simulation requires validation with analogous experimental data and observations.

Microgel regions and other structural characteristics within infinite networks at moderate to high conversion have been observed and characterized experimentally. Although formation of microgels with characteristic length scales of 50−100 nm must be preceded by single initiation events, very few experimental analyses of structural evolution at the level of individual initiation events have been demonstrated previously.

The aim of this contribution is to develop and present an experimental methodology to characterize macromolecules formed from single initiation events during homopolymerization of multifunctional monomers. The specific results relate to one monomer system with variation of two reaction conditions. In fact, the specific results are only demonstrating the true significance and innovation of this work. For the first time, a diverse set of complementary experimental tools is used together to provide information about heterogeneous features in cross-linked networks by examining size, intramolecular cross-link density, and kinetic chain length for macromolecules formed by individual initiation events.

Intramolecularly cross-linked macromolecules (ICMs) formed by very dilute initiation of pure methacrylic anhydride at various temperatures are characterized, and several questions are explored: What is the char-

[†] Department of Chemical and Biological Engineering.
[‡] Howard Hughes Medical Institute.

10.1021/ma035400w CCC: $27.50
Published on Web 04/23/2004

acteristic size of the ICMs? What influences ICM structural features such as the number of monomers incorporated and their connectivity? To address these questions, images of ICMs are captured with atomic force microscopy (AFM). Relative size information is acquired by size exclusion chromatography and dynamic light scattering. Intramolecular cross-link density is obtained from ^{1}H NMR spectroscopy. Finally, quantitative measurements of kinetic chain length are made by hydrolysis of intramolecular cross-links and analysis of the resulting linear chains by standards-calibrated gel permeation chromatography.

Temperature Effects on Homopolymerization of MA. Polymerization behavior of methacrylic anhydride has been explored by a number of other researchers.[23−26] In fact, this paper focuses on ICM formation from methacrylic anhydride because a significant body of knowledge is available for reference. In particular, methacrylic anhydride is a 1,6-diene that forms soluble chains of six-membered rings due to cyclopolymerization, or divinyl loop formation (i.e., consecutive reaction of double bonds from the same molecule during propagation of a free radical), under certain conditions.[25,26] Butler and co-workers[23] reported that cyclopolymerization is minimized, but not eliminated, at low temperature and high monomer concentration. For instance, the results of Gray and Butler indicate that only 15% of monomers form divinyl loops during low-conversion polymerization of pure MA at 0 °C and ca. 30−40% at 80 °C.[23] Although formation of intramolecular cross-links was not quantified, the results suggest that ICMs will be formed by dilute initiation in pure monomer at near-ambient temperature. Furthermore, structural differences in the ICMs are expected due to the temperature dependence of cyclopolymerization. Therefore, measurements of intramolecular cross-link density, size, and kinetic chain length were taken for various polymerization temperatures between −13 and 70 °C.

Photoiniferter-Mediated Homopolymerization of MA. Living radical initiation methods have been developed largely for monovinyl polymerizations to synthesize low-polydispersity and/or highly controlled block or graft architectures.[27−29] Controlled radical polymerizations require the formation of a dormant propagating species that becomes active for brief periods and allows insertion of monomer units before returning to a dormant state.

Researchers have attempted to use controlled radical polymerization methods during the polymerization of multifunctional monomers to facilitate more homogeneous structural evolution.[30,31] In particular, dithiocarbamyl (DTC) radicals have been implemented in living radical photopolymerizations. DTC radicals, which are relatively unreactive with polymerizable double bonds, combine with propagating carbon radicals, formed from standard photoinitiators, to produce a reinitiatable group upon exposure to UV light—a photoiniferter. Tetraethylthiuram disulfide (TED) cleaves in the presence of UV radiation to form two identical DTC radicals that subsequently impart living character to traditional photoinitated chain polymerizing systems. The final part of this contribution aims to apply the methodology for characterizing PMA ICMs to dilute homopolymerization of MA in the presence of TED to examine the effects of controlled polymerization on the ICM size and structure.

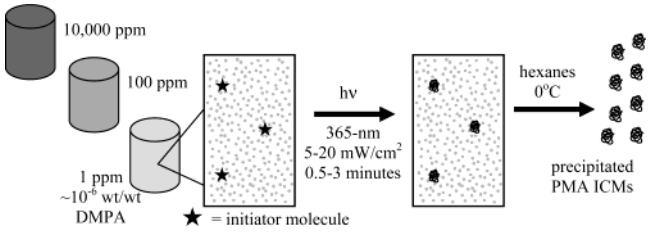

Figure 1. Schematic of ICM formation from individual initiation events. A typical concentration of photoinitiator is successively diluted to ca. 1 ppm in pure multifunctional monomer. The dilute initiator solution is exposed to 365 nm UV radiation. Finally, intramolecularly cross-linked polymer is isolated from the monomer solution by precipitation into cold hexanes.

Experimental Section

Materials. Methacrylic anhydride (MA, Aldrich Chemical Co., Milwaukee, WI) was purified by elution through a column containing basic, acidic, and neutral activated 150 mesh aluminum oxide (Aldrich) followed by vacuum distillation. 2,2-Dimethoxy-2-phenylacetophenone (DMPA), a common photoinitiator, was used as received from Ciba (trade name: Irgacure 651; Tarrytown, NY). The photoiniferter precursor, tetraethylthiuram disulfide (TED, Aldrich), was used without further purification.

Instrumentation and Methods. The initiating light source was a Novacure spot curing system with a 365 nm filter (EXFO, Mississauga, Ontario). A Digital Instruments (Santa Barbara, CA) MultiMode scanning probe microscope with a NanoScope IIIa control system was used in intermittent contact mode (TappingMode) to capture topographic images of ICMs deposited on freshly cleaved mica substrates (Ted Pella, Inc., Redding, CA). WSxM scanning probe microscopy software (Nanotec Electronica, Madrid, Spain) was used to flatten images and analyze cross sections of individual ICMs. Gel permeation chromatography (GPC) was carried out on two Waters (Milford, MA) chromatographs with 2400 series differential refractive index detectors. One GPC elutes chloroform at 1 mL/min and was calibrated against linear polystyrene or poly(methyl methacrylate) standards. The other one elutes 0.1 N $NaNO_3$ aqueous solution at 1 mL/min and was calibrated against linear poly(methacrylic acid) standards. ^{1}H NMR spectra were acquired with a Varian Inova 500 MHz spectrometer. Dynamic light scattering (DLS) was acquired with a BI-200SM goniometer (Brookhaven Instrument Corp. (BIC), Holtsville, NY) coupled with a vertically polarized, solid-state, 532 nm laser and a BI9000AT correlator. Within the BIC DLS software, a nonnegative constrained least-squares algorithm generated a multimodal distribution of effective diameters, weighted by intensity, to match the acquired correlation function. Then, a log−normal distribution was fit to the effective diameter of interest, which was found in the range 10−100 nm. Correlation functions (and subsequent data extraction) were acquired two to four times for each sample. The response for each individual sample was taken as an average of the log−normal distribution means.

Preparation of ICMs from Single Initiation Events. Figure 1 depicts the process of synthesizing individual ICMs from a very dilute solution of photoinitiator in pure MA. DMPA was successively diluted in pure MA to achieve 0.5−2 ppm (2−8 μM or 10^{-6} w/w) solutions of photoinitiator in monomer. 15−20 mL of the monomer solution was purged with argon for 30 min or more in a sealed vial. The solution was exposed to 365 nm UV radiation (5−20 mW/cm^2) for 0.5−3 min. The MA/DMPA/ICM solution was dropped slowly into 500 mL of rapidly stirring, cold hexanes. The hexanes became slightly cloudy as poly(methacrylic anhydride) (PMA) precipitated. The precipitation suspension was passed through a 0.45 μm nylon membrane to separate the precipitated PMA. The yield of precipitate was approximately 5 mg/mL of initial monomer solution, but the precipitate was not recovered quantitatively.

To prepare PMA ICMs at different temperatures, monomer solutions were purged in water or oil baths corresponding to the polymerization temperature of interest. During exposure, the vials remained partially submerged in the baths to maintain the desired temperature. Monomer solutions containing ca. 10^{-5} w/w TED in addition to DMPA were prepared by successive dilutions of TED and DMPA solutions with pure monomer.

Sample Preparation for ICM Analyses. PMA, isolated from the monomer solution, was dispersed in deuterated chloroform. After NMR analysis, the PMA ICM solution was passed through a 0.2 μm Teflon syringe filter and injected into the organic GPC. Alternatively, 1−10 mg of the isolated PMA ICMs was dispersed in ca. 1 mL of chloroform, sonicated for ca. 10 min, filtered, and analyzed by DLS. AFM sample preparation required dilution of the precipitated PMA ICMs to ca. 10 μg/mL, which was cast onto fresh mica and imaged in intermittent contact mode. Images of clean mica were captured periodically to ensure that images of ICMs were not artifacts.

Finally, 30−50 mg of the isolated PMA was stirred in ca. 1 M aqueous KOH solution for 24 h. Linear poly(methacrylic acid) (PMAA), the hydrolysis product of PMA, corresponds to the kinetic chains of the ICM samples. PMAA was made insoluble in the hydrolysis solution by adding 37% HCl (dropwise with vigorous stirring) to the hydrolysis solution, which was heated to ca. 90 °C during the precipitation step. PMAA precipitated once the solution became acidic. The precipitate was collected by centrifugation and/or filtration and redissolved in 0.1 N $NaNO_3$ for chain length analysis by the aqueous GPC.

Data Reduction. Multiple values of various responses (e.g., elution time at maximum GPC signal, mean effective diameter, etc.) at different experimental variable levels were used to compute an average (arithmetic mean) and standard deviation. The standard deviation was used to estimate the variance, and 90% confidence intervals (based on a normal distribution) were calculated for the set of responses at each variable level. The average responses and 90% confidence intervals are reported graphically. Furthermore, the number of responses used in the calculations is tabulated within each figure. No outlying responses were rejected.

Results and Discussion

Preparation of ICMs from Single Initiation Events. The photoinitiator used for this work, DMPA (as well as most other photoinitiators), cleaves into two active radicals upon photolysis. Therefore, the local environment of each initiation event contains two propagating radicals. The propagating radicals likely deactivate by a combination of one or more of three processes: (1) bimolecular termination, which could lead to covalent attachment of two ICMs created by separate radicals, (2) trapping, or (3) reaction with certain trace impurities such as oxygen. Answers to questions regarding termination events are important for understanding structural evolution of cross-linked films, but the process of exploring termination mechanisms in the conversion regime described here is nontrivial and best suited for a separate body of work. This contribution focuses on characterization of the ICMs formed from single initiation events rather than the evolution of structure from propagation of single radicals. In fact, the results mostly provide insight into the propagation events at very low conversion, which precede cross-linked network formation.

A critical assumption in the investigation of ICMs formed from single initiation events is that polymer formed from each initiation event is independent of any other initiation event. That is, the spacing between initiation events is greater than the maximum distance a propagating radical moves by reaction through unreacted double bonds. As a conservative estimate, the cumulative radicals generated for the longest exposure time was calculated, and they were all assumed to be active. Using this basis, the spacing of cumulative activated initiator was considered in checking the assumption of independent ICM formation. Specifically, eq 1 relates the fraction of initiator consumed (f_{In}) to the exposure time (t), incident light intensity (I_0), sample thickness (b), and parameters unique to the initiator molecule.

$$f_{In} = 1 - \exp[-2.303\epsilon\phi I_0 bt] \tag{1}$$

Here, ϵ is the molar extinction coefficient at the initiating wavelength, and ϕ reflects the efficiency of initiator activation after photon absorption. The maximum number of cumulative activated initiator sites was calculated for a radiation intensity ~20 mW/cm^2 (i.e., $I_0 b = 6.1 \times 10^{-8}$ quanta/(cm^2 s)), $t = 180$ s, $\epsilon \sim 150$ L/(mol cm) at 365 nm, and $\phi \sim 1$. In this case, nearly all the initiator has dissociated. The average spacing between neighboring initiators that start propagation events was calculated by assuming a uniform cubic lattice of activated initiator positions. Equation 2 relates the average initiator spacing (d_{avg}) to the fraction of activated initiators (f_{in}) and the initial initiator concentration ([DMPA]$_0$), which was approximately 4 μM.

$$d_{avg} = \left(\frac{1}{N_a f_{in}[\mathrm{DMPA}]_0}\right)^{1/3} \tag{2}$$

For the case of $f_{In} \sim 0.98$ (calculated above), $d_{avg} \sim 75$ nm. For a more common and moderate case of 1 min exposure at 10 mW/cm^2 and $\phi = 0.7$, $f_{In} \sim 0.36$ and $d_{avg} \sim 104$ nm.

The choice of initiation site spacing must be congruent with observations of propagation distances. Results to be presented in the following sections reveal that the macromolecular PMA, isolated from the monomer solution, contains ca. 4000 monomer units. The statistical solution for the average square end-to-end distance of a tetrahedrally bonded, freely rotating linear polymer chain is given by eq 3

$$\overline{r^2} = 2nl^2 \tag{3}$$

where n is the number of methylene units, and l is the length of a C−C single bond (0.154 nm).[32] For a chain containing 8000 methylene units, the end-to-end distance of the macromolecule is ~20 nm. Although this calculation is oversimplified, it indicates that the average spacing between initiation sites is likely sufficient to minimize interaction between growing ICMs due to mobility of the propagating radical by reaction through unsaturated double bonds.

Finally, translational diffusion of the growing macroradical may lead to interaction of ICMs intitiated by distinct events. On the basis of a diffusion constant estimated by the Stokes−Einstein equation, and a time for radical activity of 1 s, which is a conservative estimate because the termination mechanism is not postulated or explored, the characteristic diffusion lengths for globular structures ranging from 20 to 100 nm in MA monomer are on the order of microns. Therefore, translational diffusion of the growing macromolecules is more significant than mobility of radicals via propa-

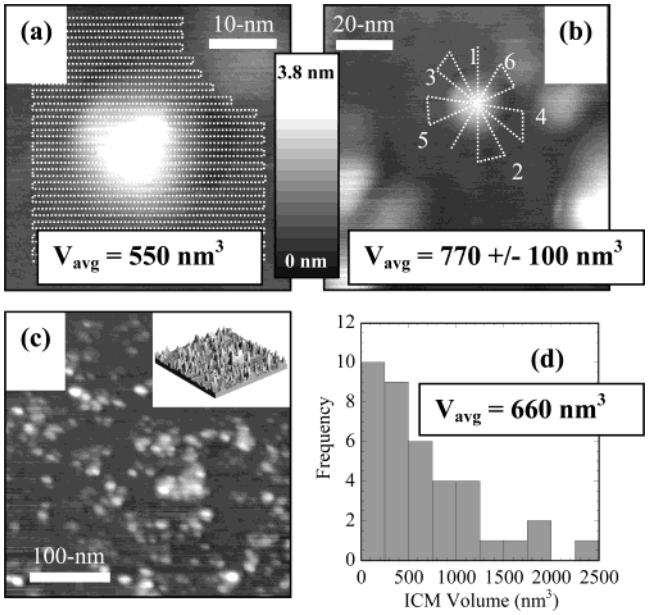

Figure 2. Direct imaging of PMA ICMs with AFM. A dispersion of PMA ICMs in chloroform is cast onto freshly cleaved mica and imaged with intermittent contact AFM. **(**a**)** The volume of a single ICM is found by analyzing evenly spaced cross sections (i.e., numerical integration). **(**b**)** For the same ICM, a volume calculation based on the assumption of a spherical cap geometry, which requires only a single cross section to measure height and diameter (eq 4), results in a volume estimate that is ca. 30% higher than the integration method. **(**c, d**)** Cross-sectional analyses of a large number of individual ICMs, followed by volume estimations using eq 4, provide information about ICM size distribution.

gation events, and it could prevent preparation of ICMs from individual initiation events. Irreversible interaction, which occurs from reaction of a growing macroradical with pendant functionality from a different ICM, will be maximized at long polymerization time (i.e., at higher concentrations of ICMs). However, experimental observations (results not shown) reveal that increased exposure time leads only to a larger sample of isolated PMA but does not affect the size of the ICMs. Furthermore, exposure time does not affect the kinetic chain length measured after hydrolysis of intramolecular anhydride cross-links. Therefore, the ICM populations formed under the experimental conditions discussed in this contribution arise from individual initiation events. Although individual ICMs likely experience physical interactions, irreversible chemical reactions between ICMs are not common. In other words, because of the low radical concentration, and resulting small number of radicals present at the periphery of ICMs, propagation to free monomer or unsaturation within ICMs occurs much more frequently than propagation to unsaturation linked to other ICMs.

Direct Observations of ICMs. Direct imaging with scanning probe microscopy yields absolute size information for isolated ICMs. Figure 2 contains images and population information from individual ICMs captured with intermittent contact AFM. Figure 2a,b details methods for calculating ICM volume from the topography information. Figure 2a shows the profiles required for numerical integration of a single ICM leading to a volume estimation of ca. 550 nm^3. The process of manually acquiring a number of evenly spaced profile lines across many individual ICMs with flat surrounding topography is not feasible for analysis of large ICM populations. Alternatively, the method used by Tomalia and co-workers[33,34] to collect volume information for dendrimeric macromolecules imaged with AFM, i.e., approximation of each ICM as a spherical cap, provides comparable volume information in a manner that facilitates analysis of a larger number of individual ICMs. Figure 2b shows six different orientations for cross-section analyses that enable estimation of ICM height and diameter. Measured diameters range from 15 to 40 nm, and heights range from 0.8 to 4.3 nm. These two parameters are used in conjunction with the solution for the volume of a spherical cap (eq 4) to estimate the ICM volume.

$$V = \frac{1}{6}\pi H\left(H^2 + \frac{3}{4}D^2\right) \tag{4}$$

The average volume was calculated as 770 nm^3, which is larger than the numerical integration approach. The uncertainty in volume calculations (±13%) due to random selection of a single orientation (e.g., in practice) was found by the standard deviation of volume estimates made using six pairs of height and diameter acquired from six different cross-section orientations. Although the assumption of spherical cap geometry leads to overestimation of the ICM volume, the assumption facilitates analysis of a large number of individual ICMs to capture the polydispersity of an ICM sample. Figure 2c depicts a large number of individual ICMs dispersed on freshly cleaved mica that are analyzed by single orientation cross-section profiling. The results of the analysis of 39 ICMs are compiled in the histogram shown in Figure 2d. More than 50% of the ICMs are between 0 and 500 nm^3, but ICMs as large as 2400 nm^3 are evident. The number-average size of the ICMs is 660 nm^3. On the basis of this average, MA monomer molecular weight (154.2 g/mol), and assuming the macromolecule density is the same as the monomer (1.035 g/mL), the average number of monomers incorporated in each ICM is ca. 2700. In fact, the true number-average size is likely smaller due to the error introduced by using eq 4 for the volume calculation of each ICM. Furthermore, results from NMR analyses indicate that unreacted monomer accounts for ca. 30−40% of the apparent number of monomers incorporated within each ICM, so the true average number of monomers within each ICM (as estimated by AFM images) is likely between 1000 and 2000. Finally, the large polydispersity reflects the nature of chain radical polymerizations of multifunctional monomers and underscores the importance of comparing average values calculated with the same basis (e.g., number-average size, in this case).

AFM is a direct measure, which under ideal conditions provides quantitative information about ICM volume without requiring calibration samples. Furthermore, AFM is the only analytical method available to measure the size of dry (i.e., nonswollen) ICMs. Unfortunately, a few drawbacks of this technique warrant consideration. First, the scanning tip has a radius of curvature on the order of nanometers. Therefore, AFM does not resolve sharp features in this size range without deconvoluting tip shape and size from characteristics of the true feature. The analysis presented in the preceding text assumes that the ICMs form low aspect ratio structure upon deposition on mica, which leads to minimal error in the estimation of volume from the raw image. The validity of this assumption has not

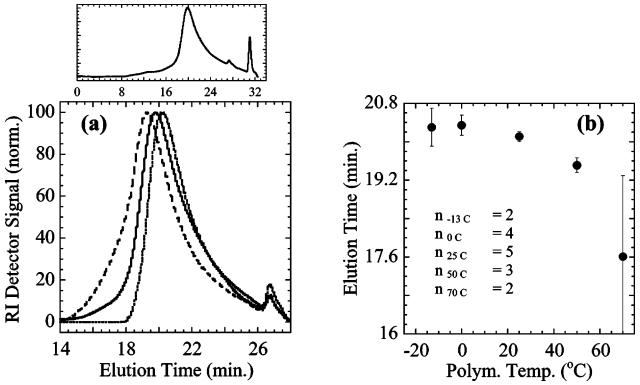

Figure 3. Size exclusion chromotography of ICMs. **(**a**)** The relative size of ICMs is measured with GPC (i.e., size exclusion principles). The top plot shows a full-scale chromatograph up to the appearance of low molecular weight components at ca. 31 min. The bottom plot contains GPC traces that reveal consistent peak shapes for samples polymerized at 0 (dotted line), 25 (solid), and 50 °C (dashed). **(**b**)** ICMs polymerized at higher temperature appear larger (i.e., shorter elution time). Error bars correspond to 90% confidence intervals, and the number of repeated samples at each temperature is indicated in the plot.

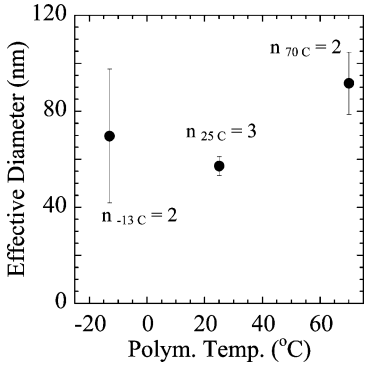

Figure 4. Dynamic light scattering of ICMs. Chloroform-dispersed ICMs are analyzed with dynamic light scattering. Large variances in the effective diameters measured at −13 and 70 °C prevent statistical significance of differences in means for each polymerization temperature. Error bars correspond to 90% confidence intervals, and the number of repeated samples at each temperature is indicated in the plot.

been investigated thoroughly, but it likely depends on ICM modulus, solvent and monomer concentration, and the interaction energy between ICMs and the mica surface. Imaging samples of ICMs with transmission electron microscopy would provide further insight into their size and geometry. Second, estimation of individual ICM volumes from an AFM image requires that cross-sectional analysis be performed on single ICMs. Lowering the concentration of ICMs in the casting solvent and selecting unaggregated features minimize the potential for inadvertently analyzing multiple ICMs with a single cross section. Finally, the technique is inefficient for examining the large sample sizes that are required to create high-resolution distributions of volume information. In particular, to explore factors such as polymerization temperature, which may have only subtle influence on the size of ICMs formed from individual initiation events, other analytical tools must be used.

Measurement of Relative ICM Size. Gel permeation chromatography (GPC) offers a facile method for characterizing populations of ICMs and relative comparison of their hydrodynamic volumes based on size exclusion principles. Normally, GPC is only applicable to soluble linear or branched polymer samples, but in this case, solvation of the ICMs facilitates comparison of elution times for samples polymerized at different temperatures. Figure 3a shows example GPC traces for ICMs formed at 0, 25, and 50 °C, and Figure 3b reports elution times corresponding to the maximum GPC detector response of PMA ICM samples polymerized at temperatures ranging from −13 to 70 °C. Although the traces shown in Figure 3a have well-resolved baselines and consistent peak shapes, the elution time at the peak maximum was used instead of the signal-averaged elution time because the baselines from a number of ICM samples were poorly defined due to low sample concentrations. All samples contained a signal at ca. 26.5 min that has not been characterized in this work.

Figure 3 reveals that increasing polymerization temperature corresponds to a decrease in elution time, i.e., an increase in the effective size based on size exclusion principles. Although the difference in elution volume between the −13 and 25 °C samples is not statistically significant, the samples polymerized at 50 and 70 °C are larger than the others with greater than 90% confidence.

Although GPC provides a qualitative tool for comparing sizes of ICMs based on size exclusion principles, this technique has some limitations. First, the presence of variable intramolecular cross-link density prevents size exclusion chromatography results from accurately reflecting the number of monomers in each macromolecule. Intramolecular cross-link density affects the apparent size of macromolecules: macromolecules containing the same number of monomers may elute differently depending upon the cross-link density.[35,36] Second, calibration standards cannot be synthesized for different cross-linking monomers with variable degrees of cross-link density, so all information is limited to relative comparisons. Nonetheless, GPC provides important comparative information and can be validated by other methods, such as light scattering.

Light scattering is ideally suited to characterize size and shape factors of macromolecules in dilute solution. Dynamic light scattering monitors Brownian diffusion of small particles and reports the distribution of effective diameters that matches the measured diffusion characteristics. Figure 4 contains results of DLS measurements of PMA ICMs dispersed in chloroform. The average effective diameters of ICM populations are plotted for three polymerization temperatures: −13, 25, and 70 °C. Although the inconsistency in repeated measurements of the low-temperature sample detracts from statistical significance of the difference in means, the results in Figure 4 (i.e., average effective diameters of ICMs) for 25 and 70 °C support the general trend of increasing size with increasing polymerization temperature as reported in Figure 3.

Rigorous examination of ICMs by light scattering is beyond the scope of this contribution. Because of the variable cross-link density, unknown degree of swelling, and uncharacterized shape factors of the ICMs, the absolute value of the effective diameter has diminished significance for determination of a characteristic size of structural evolution from individual initiation events. Nonetheless, comparison of measured effective diameters for ICM samples prepared with different polymerization conditions validates the body of relative size information collected with GPC.

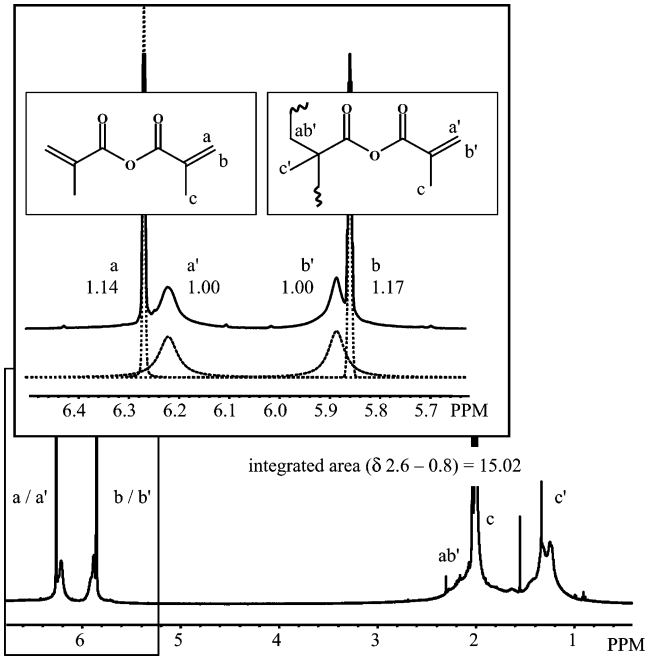

Figure 5. Intramolecular cross-link density measured with ^{1}H NMR. Relative amounts of unreacted, singly reacted, and doubly reacted methacrylic anhydride are found by deconvolution of the overlapping signals from pendant and monomeric vinyl protons (expanded view), followed by integration of the region between 0.8 and 2.5 ppm that contains signals from methyl (c and c′) and methylene (ab′) protons.

The apparent increase in size of the ICMs as a function of temperature can be attributed to a number of factors. For instance, the reactivity of the methacrylic double bonds increases with temperature as do the mobilities of monomers, macromolecules, and segments. These factors contribute to a higher effective reactivity of propagating radicals. However, the effect of increased reactivity of propagating radicals on the formation of intramolecular cross-links cannot be determined a priori. Better understanding of the effect of temperature on the evolution of ICMs from individual initiation events necessitates further exploration of cross-link density.

Measurement of Intramolecular Cross-Link Density. To measure the fraction of doubly reacted monomers (i.e., intramolecular cross-link density), distinguishing between monomeric and pendant unsaturation is critical. Quantitative removal of unreacted monomer from within the intramolecularly cross-linked structures is not trivial. Repeated dissolution and precipitation of the ICM samples resulted in lowering the monomer fraction, but not completely eliminating it (results not shown), at the expense of a dramatically reduced sample mass. Fortunately, for the case of PMA, the monomer is sufficiently compact that reaction of one end creates an apparent chemical shift in the ^{1}H NMR signal of the pendant double bond, which is likely due to dipolar coupling. Figure 5 contains a representative ^{1}H NMR spectrum of a sample of PMA ICMs solvated with deuterated chloroform. The figure also shows an expanded view of the unsaturated methylene peak region (i.e., 5.5−6.5 ppm) from a sample of PMA ICMs containing unreacted MA monomer. Deconvolution of the four distinct peaks indicates that the PMA ICM sample contains 0.36 mol of unreacted monomer per mole of singly reacted monomer. In particular, the narrow peak centered at 6.27 ppm (labeled "a" in Figure 5) corresponds to a monomeric proton in the cis position relative to the anhydride group. The broad signal centered at 6.22 ppm corresponds to the same proton position (a′) for a monomer that has been polymerized on the opposite side of the anhydride linker (resulting in a pendant double bond). Likewise, the signals at 5.89 and 5.86 ppm correspond to protons trans to the anhydride that are pendant (b′) and monomeric (b), respectively. Both groups (a/a′ and b/b′) provide the exact same quantitative information. The ratio of singly reacted monomers to unreacted monomers is calculated from the areas of the deconvoluted signals. In this case, 0.57 mol of unreacted monomer (e.g., 1.14 divided by two double bonds per monomer) is present for each 1.00 mol of singly reacted monomer in the sample. Finally, the relative number of moles of doubly reacted monomer is calculated from the methyl group signals (c and c′) and reacted methylene signals (ab′), which appear between 0.8 and 2.6 ppm. Specifically, the relative signal from six protons associated with both methyl groups in each unreacted monomer (e.g., $6 \times 0.57 = 3.42$) and eight protons associated with two methyl groups and one methylene group in each singly reacted monomer (e.g., $8 \times 1.00 = 8.00$) are subtracted from the integrated region between 0.8 and 2.6 ppm. The remaining signal corresponds only to 10 protons associated with doubly reacted monomer. Therefore, the relative amounts of unreacted, singly reacted, and doubly reacted monomers are known, and the fraction of doubly reacted monomers is found.

In the case of MA, the unique structure facilitates deconvolution of monomer and polymer ^{1}H NMR signals. However, to generalize this method for determining the fraction of doubly reacted monomers in other monomer systems, further deconvolution of peaks other than the unsaturated methylene peaks is necessary. In particular, higher resolution NMR techniques, relaxation time experiments, and/or ^{13}C NMR (i.e., cross-polarization magic angle spinning, CPMAS) must be implemented because chemical shift differences in ^{1}H NMR will most likely not be found in monomers with longer (unconjugated) links between functional groups. Furthermore, extension of this method to tri- or higher multivinyl monomers will not be trivial because of the larger number of possible reacted states (e.g., unreacted, singly reacted, doubly reacted, triply reacted, etc.).

Figure 6 summarizes the results of the measured fraction of doubly reacted methacrylic anhydride (ρ_{DR}), i.e., cross-link density, for PMA ICM populations created between −13 and 70 °C. The average value of the measured intramolecular cross-link density increases with increasing polymerization temperature from 0 to 70 °C. The fraction of doubly reacted monomers per total monomers reacted for the PMA ICMs varies from 25 to 45%, albeit with large uncertainty. Furthermore, intramolecular cross-links and divinyl loops cannot be distinguished in the NMR spectra, so the fraction of doubly reacted monomers includes monomers that have cyclopolymerized to form divinyl loops. Divinyl loops do not inhibit chain extension in good solvents, but intramolecular cross-links do affect ICM solvation and/or extension. The unfilled symbols in Figure 6 represent the fractions of doubly reacted monomers that serve as intramolecular cross-links, after subtraction of the amount of divinyl loops (predicted from experimental results of other authors[23,24] at the different polymerization temperatures) from the measured data (filled

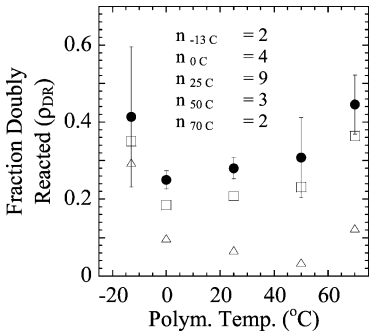

Figure 6. Temperature dependence of intramolecular cross-link density. Results of ^{1}H NMR analyses to determine the fraction of doubly reacted monomers (i.e., doubly reacted relative to the sum of singly and doubly reacted monomers) are reported as a function of polymerization temperature. Polymerization temperature does not have a significant effect on the measured intramolecular cross-link density (solid circles). Error bars correspond to 90% confidence intervals, and the number of repeated samples at each temperature is indicated in the plot. The fraction of divinyl loops formed at each experimental temperature is subtracted from the measured fraction of doubly reacted monomers to indicate the fraction of doubly reacted monomers that inhibit chain extension. Estimates of divinyl loop concentration were found empirically from two sources. The corrected data are reported as unfilled squares[24] and unfilled triangles.[23]

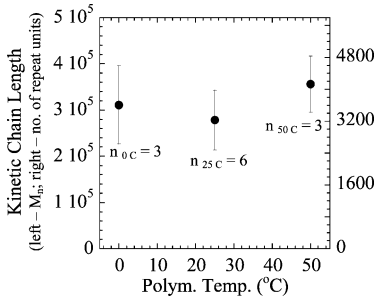

Figure 7. Effect of polymerization temperature on kinetic chain length. Kinetic chain lengths, measured by degradation of PMA ICMs to linear poly(methacrylic anhydride) chains and quantified by calibrated GPC, are not affected significantly by varying polymerization temperature. The left axis reports number-average molecular weight (M_n), and the right axis simply changes the same data to the number of repeat units (i.e., the number of double bonds reacted by a propagating radical). Error bars correspond to 90% confidence intervals, and the number of repeated samples at each temperature is indicated in the plot.

symbols). Square symbols represent corrections based on experiments reported by Matsumoto and co-workers,[24] and triangular symbols represent correction of the measured fraction of doubly reacted monomers with data published by Gray and Butler.[23] Although both suggest that divinyl loop formation increases with temperature, the empirical predictions of divinyl loop formation differ significantly in the low-temperature range. According to the temperature dependence of divinyl loop formation reported by Gray and Butler,[23] the intramolecular cross-link density (i.e., the fraction of doubly reacted monomers not including divinyl loops) decreases with increasing polymerization temperature. Intramolecular cross-links will affect the apparent size of solvated ICMs because they will restrict full extension in a good solvent. In fact, the ambiguity in the observed and calculated effects of polymerization temperature on the fraction of doubly reacted monomers, particularly with respect to ICM size, necessitates further exploration of the ICM structure—namely, measurement of the kinetic chain lengths (i.e., the number of double bonds reacted by each propagating radical).

Determination of Kinetic Chain Lengths. The number of monomer molecules incorporated into an ICM relates to the kinetic chain length of the propagating radicals. After hydrolysis of the anhydride cross-links in the PMA ICMs, the isolated linear PMAA chains were analyzed quantitatively by GPC in conjunction with PMAA calibration standards. Figure 7 shows the kinetic chain lengths, calculated by integration of the number-average molecular weight distribution, for samples of PMA ICMs polymerized at 0, 25, and 50 °C. Interestingly, no statistical difference in kinetic chain length was observed by changing polymerization temperature in this range. The overall average PMAA chain length ($\overline{M_n}$) is ca. 3.0×10^5, which corresponds to propagation of the active radical through ca. 3500 methacrylic double bonds.

Internal Consistency of Various Methods. The kinetic chain length analysis results in an absolute measure of the number of double bonds reacted by a propagating radical. Therefore, combination of the kinetic chain length analysis with information about intramolecular cross-linking density, acquired with ^{1}H NMR, yields an absolute value for the number of monomer units incorporated into each ICM. Equation 5 relates the total number of monomers (N) reacted by a single radical to the kinetic chain length (ν) and intramolecular cross-linking density (ρ_{DR}) for a divinyl monomer system.

$$N = \frac{\nu}{1 + \rho_{DR}} \tag{5}$$

For the PMA system discussed in this contribution, each radical reacts with ca. 3000 monomers, and samples from each of the polymerization temperatures are the same within experimental uncertainty. The value agrees reasonably with the value for the number of monomers calculated from AFM observations of individual ICMs formed at 25 °C. In fact, agreement between the independent measures of N provides partial validation of both procedures to find N. The agreement also suggests that each initiation event, which produces two propagating radicals, produces two independent ICMs. Information about N, the number of monomers per ICM (or propagating radical), is particularly valuable because it can be compared to ICMs formed via alternative reactant and reaction parameters, and it is highly complementary with information acquired from simulations of multifunctional monomer polymerizations.

Combination of kinetic chain length and intramolecular cross-link density measurements to find the number of monomers incorporated in ICMs polymerized at different temperatures reveals that the apparent increase in ICM size shown by size exclusion chromatography and light scattering was not a result of more monomers being incorporated at higher polymerization temperatures. However, an ICM with a more open structure due to lower intramolecular cross-link density (i.e., after subtraction of divinyl loop formation) will appear larger when solvated by a good solvent or monomer.[36] Thus, the apparent size increase as a function of polymerization temperature may be reflective of increased solvation of the ICMs with lower intramolecular cross-link density (i.e., larger divinyl loop

Table 1. Investigation of ICMs Formed during Photoiniferter-Mediated Homopolymerization of Methacrylic Anhydride

evaluation metric	no TED[a]	1×10^{-5} w/w TED[a]	qualitative result
elution time (min)	18.65 ± 0.08 ($n = 2$)	18.84 ± 0.02 ($n = 2$)	increases
effective diameter (nm)	57.2 ± 3.9 ($n = 3$)	41.0 ± 3.9 ($n = 4$)	decreases
fraction doubly reacted	0.279 ± 0.027 ($n = 9$)	0.444 ± 0.120 ($n = 3$)	increases
kinetic chain length ($\times 10^{-5}$)	2.78 ± 0.65 ($n = 6$)	1.60 ± 0.06 ($n = 2$)	decreases

[a] The reported uncertainties correspond to 90% confidence intervals, and the numbers of samples are shown in parentheses.

fractions). Overall, the internal consistency of the various techniques for characterization of the ICMs formed from individual initiation events indicates that the methodology will provide useful information about structural evolution, particularly effects of reaction and reactant parameters on the structural evolution of PMA and other multifunctional monomers.

Investigation of Photoiniferter-Mediated Homopolymerization of MA. Other authors[30,31] have explored multifunctional monomer polymerizations in the presence of photoiniferters. They hypothesized that a more homogeneous structure would be formed due to the living character imparted by the iniferter. Investigation of ICMs formed at very low conversion during iniferter-mediated homopolymerization of methacrylic anhydride may provide insight into the effects of the living radical initiator on homogeneity of the macroscopic network.

First of all, the "living" character of a photoiniferter-mediated polymerization was explored. In theory, the dithiocarbamyl (DTC) radicals, generated when TED cleaves due to UV light absorption, repeatedly recombine with propagating radicals and cleave upon further exposure to decrease the rate of propagation and consequently increase the homogeneity of individual kinetic chains. Therefore, we hypothesized that exposure time affects the properties, particularly size, of ICMs formed in the presence of TED. However, no difference in ICM size was observed for samples prepared with different exposure times ranging from 1 to 5 min (results not shown). This result suggests that the possibility for reinitiation of the propagating chain end is lost in this particular experiment. It also indicates that an irreversible termination event must be occurring simultaneously. For example, the propagating radicals could be terminated with oxygen molecules or other radical scavenging impurities at relatively early stages of the ICM formation process.

The properties of ICMs formed in the presence of TED were compared to properties of ICMs synthesized without the photoiniferter precursor to gain insight into the actual effect of photoiniferter-mediated polymerization on polymer formed from individual initiation events. Table 1 contains ICM size comparisons and results from measurement of cross-link density and kinetic chain length for PMA ICMs prepared at 25 °C without TED and in the presence of ca. 10^{-5} w/w TED (i.e., 10 times excess relative to the photoinitiator). TED has a slightly higher molar absorptivity than DMPA at 365 nm (210 and 160 L/(mol cm), respectively[17]). Although the efficiency of radical formation is not well-known for either compound, the concentration of DTC radicals was approximately 1 order of magnitude higher than the concentration of propagating radicals throughout the exposure time.

Table 1 reveals that ICMs synthesized in the presence of TED exhibit longer GPC elution times than ICMs prepared with only photoinitiator. This result suggests that photoiniferter mediation leads to smaller ICMs. Please note values of GPC elution times differ from those reported in Figure 3 because the chromatography columns were replaced between the variable polymerization temperature experiments and the TED study. The dynamic light scattering results shown in Table 1 support the GPC results, which suggest that dilute initiation of MA in the presence of TED results in smaller ICM formation. In addition, results of intramolecular cross-link density (ρ_{DR}) measurements are shown in the table. Interestingly, the addition of TED appears to increase the fraction of doubly reacted monomers. An increase in cross-linking density due to TED cannot be rationalized with first principles. In fact, this interesting result highlights the unique information provided by this methodology, and it provides motivation for continued exploration of photoiniferter-mediated homopolymerizations of multifunctional monomers. Finally, Table 1 contains results of kinetic chain length measurements. The kinetic chains for ICMs prepared by iniferter-mediated polymerization are shorter than those from ICMs synthesized without TED. This result, in conjunction with the increase of cross-link density, validates the results from GPC and DLS: Photoiniferter-mediated polymerization of MA produces ICMs that are ca. 30% smaller than ICMs formed by traditional photoinitiation. In addition to fewer monomers being incorporated in the ICMs, the increase in intramolecular cross-link density may be responsible for the smaller apparent size because chain solvation is limited to a larger degree than it is in ICMs synthesized without TED.

Finally, with respect to previous investigations,[30,31] the "living" character of the photoiniferter-mediated polymerization is lost due to irreversible termination of the propagating radicals with impurities or severe local diffusion limitations that reduce or eliminate the reinitiation character of the photoiniferter-mediated system. Therefore, the "living" character is probably not responsible for increased film homogeneity, but the decrease in size of the ICMs formed at very low conversion could lead to a final network with more homogeneous nano- or microstructural components.

Acknowledgment. The authors thank Profs. Dan Schwartz (Chemical Engineering), Kathy Rowlen (Chemistry), and Kathy Nagy (Geology) and their groups for assistance in acquiring AFM images. Also, the authors are grateful to Prof. Ted Randolph (Chemical Engineering) for availability of the light scattering instrument(s) and Rich Shoemaker (Chemistry) for providing NMR expertise. The authors thank the I/UCRC for Fundamentals and Applications of Photopolymerizations for financial support and feedback on technical content. Furthermore, NSF and Department of Education GAANN fellowships to J.B.H. are gratefully acknowledged.

References and Notes

(1) Dusek, K. *Polym. Gels Networks* **1996**, *4*, 383−404.

(2) Kloosterboer, J. G.; van de Hei, G. M. M.; Boots, H. M. J. *Polym. Commun.* **1984**, *25*, 354−357.
(3) Kloosterboer, J. G. *Adv. Polym. Sci.* **1988**, *84*, 1−61.
(4) Podalinskii, A. V. *Vysokomol. Soedin., Ser. A* **1974**, *16*, 2758−2764.
(5) Bowman, C. N.; Peppas, N. A. *Chem. Eng. Sci.* **1992**, *47*, 1411−1419.
(6) Anseth, K. S.; Bowman, C. N. *J. Polym. Sci., Part B: Polym. Phys.* **1995**, *33*, 1769−1780.
(7) Cook, W. D. *J. Appl. Polym. Sci.* **1991**, *42*, 2209−2222.
(8) Kloosterboer, J. G.; Lijten, G. *Polymer* **1990**, *31*, 95−101.
(9) Scranton, A. B.; Bowman, C. N.; Klier, J.; Peppas, N. A. *Polymer* **1992**, *33*, 1683−1689.
(10) Lungu, A.; Neckers, D. C. *J. Polym. Sci., Part A: Polym. Chem.* **1996**, *34*, 3355−3360.
(11) Berlin, A. A.; Matvejeva, N. G. *Macromol. Rev., Part D: J. Polym. Sci.* **1980**, *15*, 107−206.
(12) Allen, P. E. M.; Bennett, D. J.; Hagias, S.; Hounslow, A. M.; Ross, G. S.; Simon, G. P.; Williams, D. R. G.; Williams, E. H. *Eur. Polym. J.* **1989**, *25*, 785−789.
(13) Sellergren, B.; Ruckert, B.; Hall, A. *Adv. Mater.* **2002**, *14*, 1335−1335.
(14) Sellergren, B.; Ruckert, B.; Hall, A. J. *Adv. Mater.* **2002**, *14*, 1204-+.
(15) Wen, M.; McCormick, A. V. *Macromolecules* **2000**, *33*, 9247−9254.
(16) Rey, L.; Duchet, J.; Galy, J.; Sautereau, H.; Vouagner, D.; Carrion, L. *Polymer* **2002**, *43*, 4375−4384.
(17) Lovell, L. G.; Elliott, B. J.; Brown, J. R.; Bowman, C. N. *Polymer* **2001**, *42*, 421−429.
(18) Lungu, A.; Neckers, D. C. *Macromolecules* **1995**, *28*, 8147−8152.
(19) Allen, P. E. M.; Simon, G. P.; Williams, D. R. G.; Williams, E. H. *Eur. Polym. J.* **1986**, *22*, 549−557.
(20) Allen, P. E. M.; Simon, G. P.; Williams, D. R. G.; Williams, E. H. *Macromolecules* **1989**, *22*, 809−816.
(21) Anseth, K. S.; Bowman, C. N. *Chem. Eng. Sci.* **1994**, *49*, 2207−2217.
(22) Hutchison, J. B.; Anseth, K. S. *Macromol. Theory Simul.* **2001**, *10*, 600−607.
(23) Gray, T. F.; Butler, G. B. *J. Macromol. Sci., Chem.* **1975**, *A9*, 45−82.
(24) Matsumoto, A.; Terada, T.; Oiwa, M. *J. Polym. Sci., Part A: Polym. Chem.* **1987**, *25*, 775−781.
(25) Butler, G. B. *Acc. Chem. Res.* **1982**, *15*, 370−378.
(26) Butler, G. B.; Matsumoto, A. *J. Polym. Sci., Part C: Polym. Lett.* **1981**, *19*, 167−176.
(27) Davis, K. A.; Matyjaszewski, K. In *Statistical, Gradient, Block and Graft Copolymers By Controlled/Living Radical Polymerizations*; Springer-Verlag: Berlin, 2002; Vol. 159, pp 1−169.
(28) Coessens, V.; Pintauer, T.; Matyjaszewski, K. *Prog. Polym. Sci.* **2001**, *26*, 337−377.
(29) Hawker, C. J.; Bosman, A. W.; Harth, E. *Chem. Rev.* **2001**, *101*, 3661−3688.
(30) Kannurpatti, A. R.; Lu, S. X.; Bunker, G. M.; Bowman, C. N. *Macromolecules* **1996**, *29*, 7310−7315.
(31) Kannurpatti, A. R.; Anderson, K. J.; Anseth, J. W.; Bowman, C. N. *J. Polym. Sci., Part B: Polym. Phys.* **1997**, *35*, 2297−2307.
(32) Flory, P. J. *Principles of Polymer Chemistry*; Cornell University Press: Ithaca, NY, 1953.
(33) Li, J.; Swanson, D. R.; Qin, D.; Brothers, H. M.; Piehler, L. T.; Tomalia, D.; Meier, D. J. *Langmuir* **1999**, *15*, 7347−7350.
(34) Li, J.; Piehler, L. T.; Qin, D.; Baker, J. R.; Tomalia, D. A.; Meier, D. J. *Langmuir* **2000**, *16*, 5613−5616.
(35) Davankov, V. A.; Ilyin, M. M.; Tsyurupa, M. P.; Timofeeva, G. I.; Dubrovina, L. V. *Macromolecules* **1996**, *29*, 8398−8403.
(36) Mecerreyes, D.; Lee, V.; Hawker, C. J.; Hedrick, J. L.; Wursch, A.; Volksen, W.; Magbitang, T.; Huang, E.; Miller, R. D. *Adv. Mater.* **2001**, *13*, 204−208.

MA035400W